J Inorg Organomet Polym (2016) 26:819–828
DOI 10.1007/s10904-016-0385-8

Preparation of a Novel Nano-scale Lead (II) Zig-Zag Metal–Organic Coordination Polymer with Ultrasonic Assistance: Synthesis, Crystal Structure, Thermal Properties, and NBO Analysis of $[Pb(\mu\text{-}2\text{-}pinh)N_3\ H_2O]_n$

Babak Mirtamizdoust[1] · Dariusz C. Bieńko[2] · Younes Hanifehpour[3] · Edward R. T. Tiekink[4] · Veysel T. Yilmaz[5] · Pejman Talemi[6] · Sang Woo Joo[3]

Received: 23 February 2016 / Accepted: 3 May 2016 / Published online: 12 May 2016

Abstract A novel nano-cauliflower-shaped lead(II) metal–organic coordination polymer, $[Pb(\mu\text{-}2\text{-}pinh)N_3\ H_2O]_n$ (**1**), was synthesized using an ultrasonic method. The nanostructure was characterized by scanning electron microscopy (SEM), X-ray powder diffraction, IR spectroscopy, elemental analysis, and thermal analysis. The compound was structurally characterized by single-crystal X-ray diffraction. The coordination compound takes the form of a zig-zag one-dimensional polymer in solid state. The coordination number of the lead(II) ions is six (PbN_4O_2) with three nitrogen atoms and one oxygen atom from two linker organic ligands, as well as one oxygen from coordinated water and one nitrogen atom from terminal coordinated azide anion. It has a stereo-chemically active lone electron pair, and the coordination sphere is hemidirected. The zig-zag 1D chains interact with neighbouring chains through weak interactions, creating a 3D supramolecular metal–organic framework. Lead oxide nanoparticles were obtained by thermolysis of the new nano coordination compound at 180 °C with oleic acid as a surfactant. The morphology and size were further studied using SEM. Natural bond orbital analyses demonstrate the electronic properties of the lead centre and other atoms.

Keywords Nano zig-zag polymer · Nano metal–organic coordination compound · NBO analysis · Lead(II) nanoparticle

✉ Babak Mirtamizdoust
babakm.tamizdoust@gmail.com

✉ Younes Hanifehpour
y_hanifehpour@yu.ac.kr

✉ Sang Woo Joo
swjoo1@gmail.com

[1] Department of Chemistry, Faculty of Science, University of Qom, PO Box 37185-359 Qom, Iran

[2] Faculty of Chemistry, Wrocław University of Technology, Wybrzeże Wyspiańskiego 27, ul Smoluchowskiego 23, 50-370 Wrocław, Poland

[3] School of Mechanical Engineering, WCU Nano Research Center, Yeungnam University, Gyongsan 712-749, South Korea

[4] Research Centre for Crystalline Materials, Faculty of Science and Technology, 47500 Bandar Sunway, Selangor Darul Ehsan, Malaysia

[5] Department of Chemistry, Faculty of Arts and Sciences, Uludag University, 16059 Bursa, Turkey

[6] School of Chemical Engineering, University of Adelaide, Adelaide, SA 5005, Australia

1 Introduction

Recently, metal–organic coordination polymers have attracted interest due to the diverse structural motifs and useful potential properties [1, 2]. Numerous factors affect the assembly of these coordination polymers, such as the coordination configuration of metal ions, geometric characteristics of organic ligand spacers, metal–ligand ratios, solvents, counter-anion characteristics, and reaction conditions [3–7]. Because of their economic, environmental, and biological roles, the selective sensing and chelation of toxic heavy metals such as Pb(II), Cd(II), and Hg(II) is very important. Lead is still the most commonly encountered toxic metal pollutant in the environment. The unique coordination chemistry of Pb(II) can be exploited to develop practical ligands as extractants, lead-poisoning treatments, and sensors [8–10].

The chemistry of lead(II) coordination frameworks has attracted great interest because of its large ion radius,

variable coordination number, the possibility of a stereochemically active lone pair of $6s^2$ outer electrons, novel network topologies, and interesting properties [11]. Lead(II) has an electronic structure of $[Xe]4f^{14}5d^{10}6s^2$. The 6*s* orbital contracts and stabilizes due to relativistic effects that are strongest in Au(I) but also occur in close 6*p* metals such as lead. This stabilized 6*s* pair participates less in the chemistry of the element by becoming an "inert pair," which explains why inorganic lead forms compounds in a lower oxidation state (less by two) than expected from its group number [12, 13]. This may also affect the stereochemistry of lead(II)-organic coordination compounds.

This influence can be understood in terms of simple hybridization or valence shell electron-pair repulsion [14]. In spite of its stabilization, it seems that the 6*s* orbital can hybridize with the 6*p* orbitals to give a "stereochemically active" 6*s* electron pair [or stereochemically active lone electron pair (*SALEP*)], which occupies one position in the coordination sphere of the metal. Considering that the pair is not directly detectable, its presence is normally identified by a void in the distribution of the coordination bonds (*hemidirected* coordination; see scheme 1). In the absence of hybridization, the pair exhibits only *s* character, which makes it "stereochemically inactive." Thus, the complex does not show a gap or void in the bond distribution (*holodirected* coordination; see Scheme 1) [12].

In contrast to the usual hybrid metal–organic coordination compounds, there are very few reports on the synthesis of nano metal–organic coordination polymers. Another application that has not yet been investigated thoroughly is the use of organic–inorganic coordination polymers as precursors for the preparation of inorganic nano compounds [15, 16]. Theoretical methods such as DFT calculations can be used to find energy minima, determine structures, and predict the spectroscopic and electronic properties of the compounds, and the results can be compared with experimental data for verification [18–21]. However, there are only a few reports on theoretical calculations for the properties of lead(II) complexes.

Our research group has intensively focused on the synthesis and characterization of lead(II) complexes and their metal organic coordination polymers [22–33]. One of the tools that we have used in this work is sonochemistry, in which chemical reactions are influenced by the application of ultrasound (20 kHz–10 MHz). The application of ultrasound in synthetic organic chemistry has received attention because ultrasonic waves in liquids cause chemical reactions in homogeneous and heterogeneous systems [17]. As a continuation of previous studies, we report the first synthesis of lead(II) metal–organic coordination polymers with an azido terminal ligand in the presence of 2-pyridinecarbaldehyde isonicotinoylhydrazone (H-2-pinh) Schiff-base ligand. We also report the first natural bond orbital (NBO) analysis study of lead(II)-azide complexes and describe a simple sonochemical synthesis method for nano-structures of this coordination polymer and its use in the preparation of PbO nanoparticles.

2 Results and Discussion

The reaction between the H-2-pinh ligand with a solution of lead(II) acetate and sodium azide led to the formation of the new lead(II) coordination polymer, $[Pb(\mu\text{-}2\text{-pinh})N_3\ H_2O]_n$ (**1**). Nano-cauliflower shapes of compound **1** were obtained by applying ultrasound to a methanolic solution, and single-crystalline material samples were obtained by applying a heat gradient to a solution of the reagents (the branched tube method [34]). There are very few reports on the synthesis of nano-cauliflower shape compounds [50–52].

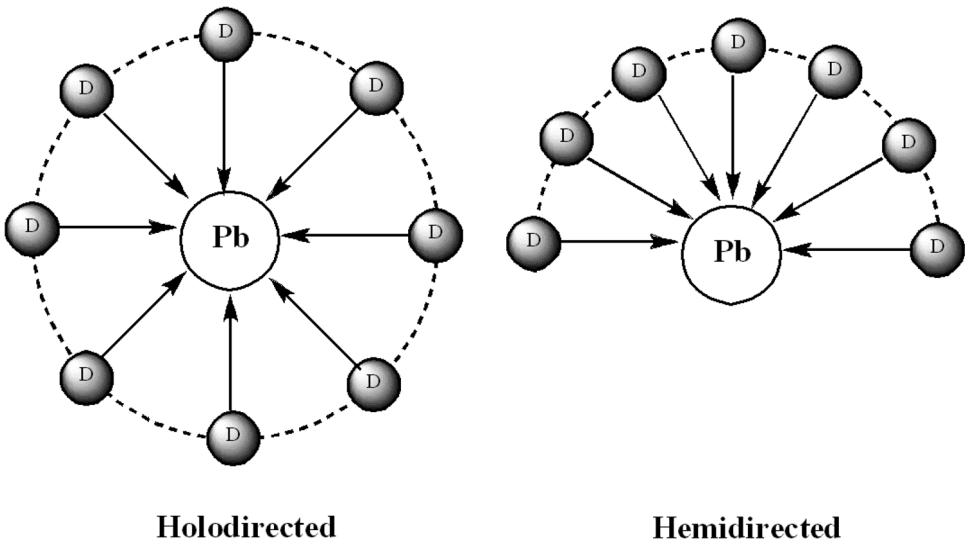

Scheme 1 Stereochemical influence of the 6*s* pair on coordination sphere (*D* donor atom of a ligand)

Scheme 2 gives an overview of the two different routes used for the synthesis of $[Pb(\mu\text{-}2\text{-pinh})N_3\ H_2O]_n$ (**1**):

The elemental analysis and IR spectra results of the nanostructures and the single-crystalline material are indistinguishable. The IR spectra of the nanostructures and the single-crystalline materials and calculated IR show the characteristic absorption bands of the 2-pinh ligand (Fig. 1). The relatively weak band around 3064 cm^{-1} is attributed to the absorption of the aromatic CH hydrogen atoms. The absorption band in the frequency range of 1499–1634 cm^{-1} corresponds to the vibrations of aromatic rings of the 2-pinh ligand. The absorption bands with strong intensity at 1460 cm^{-1} correspond to the C=N bond of the imine group of the ligand. The strong band at 2021 cm^{-1} corresponds to N_3^- anions [35].

Figure 2 shows the calculated Powder XRD from a crystal cell (Fig. 2a) and a comparison with the Powder XRD pattern of a typical sample of **1** prepared by the sonochemical process (Fig. 2b). Acceptable matches with slight differences in 2θ were observed between the calculated and experimental powder X-ray diffraction patterns (Fig. 2b). The significant broadening of the peaks indicates that the particles have nanometer dimensions. This was estimated using the Scherrer formula, $D = 0.891\lambda/\beta\cos\theta$, where D is the average grain size, λ the X-ray wavelength (0.15405 nm), and θ and β are the diffraction angle and full-width at half maximum of an observed peak, respectively. The average grain size was 30 nm. Compound **1** prepared by the sonochemical method shows interesting morphology comprising sheet-like structures with an approximate thickness of 30 nm (Fig. 3).

The formation mechanism of this structure needs further investigation. It may be a result of the packing of the crystal structure on a molecular level (see Fig. 9), which might have influenced the morphology. Single-crystal X-ray structure determination reveals that **1** has the stoichiometry of $[Pb(\mu\text{-}2\text{-pinh})N_3(H_2O)]_n$. Figure 4 shows the asymmetric unit and atom numbering scheme, while Table 1 presents the crystal data and structure refinement details.

These data indicate that the lead atom is chelated by one oxygen and two nitrogen atoms of the 2-pinh ligand. It is also coordinated by the pyridyl-N4 atom of a neighbouring molecule to generate a zigzag chain along the c-axis (Fig. 5a). Thus, the 2-pinh ligand is tetradentate. The lead atom is also coordinated by a water molecule and the N5 atom of a terminally bound azide. The water molecule and donor atoms from the 2-pinh ligands occupy an approximate plane with the azide N5 atom lying to one side. To the other side is a weakly connected N3 atom that is otherwise not involved in coordination such that the zigzag chains are linked into double chains (Fig. 5b). As shown in Fig. 6, the lead atom is seven-coordinated, and a relatively large void is apparent on the same side of the N3O2 plane as the N3 atom. The coordination geometry is based on a Ψ-dodecahedron.

Figure 7 shows the unit cell contents. The double layers demonstrated in Fig. 5b stack along the a-axis and are connected in a three-dimensional architecture by O1w–H···N3 hydrogen bonds. This indicates that this atom is pivotal in ensuring the cohesiveness of the crystal (O1w–$H\cdots N3^{iii}$ = 2.26 Å; $O1w\cdots N3^{iii}$ = 3.049(8) Å and angle at

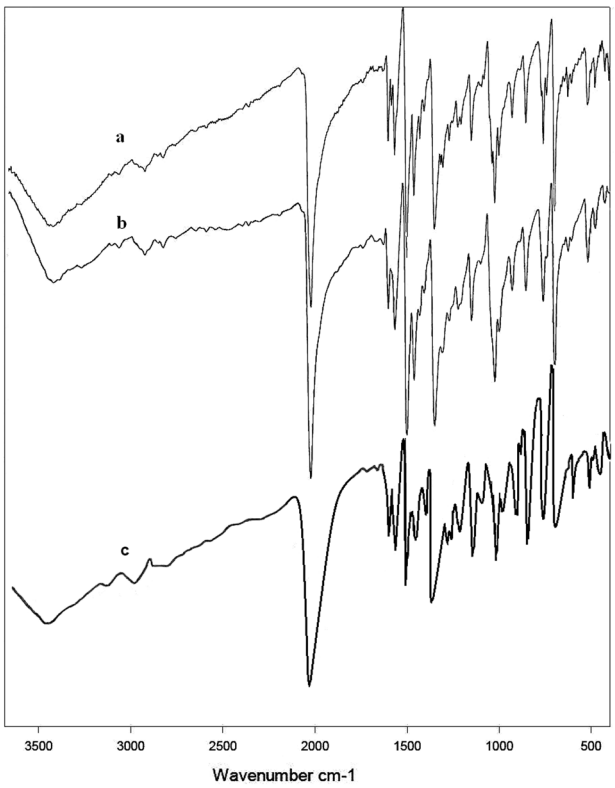

Fig. 1 The FT-IR spectra of **1** (*a* nanostructures, *b* single-crystalline, *c* calculated)

Scheme 2 Materials produced and synthetic methods

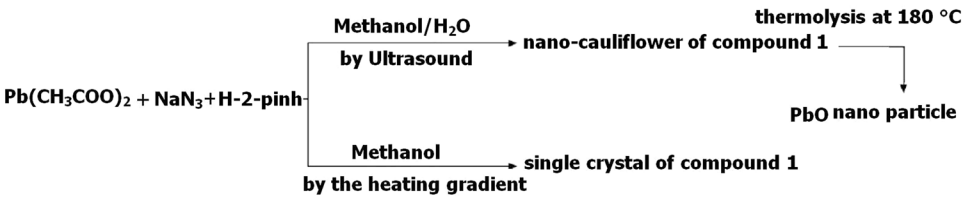

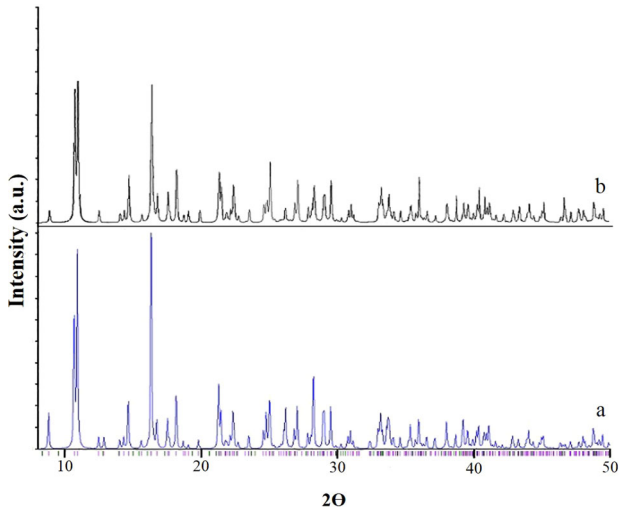

Fig. 2 *a* calculated Powder XRD from a crystal cell and *b* powder XRD from nano-structure of compound **1**

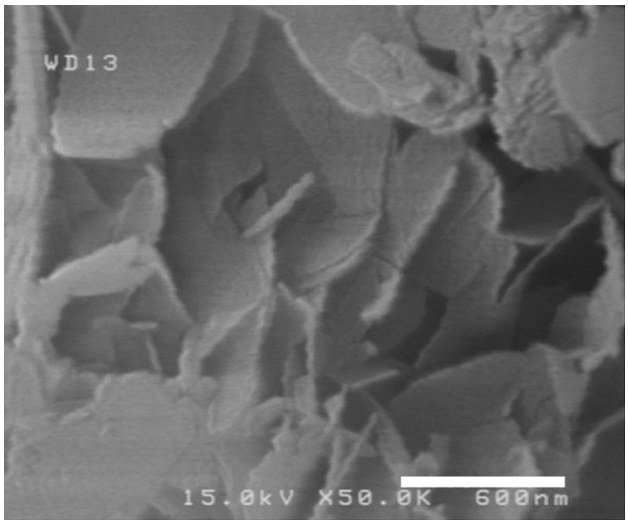

Fig. 3 SEM image of $[Pb(\mu\text{-}2\text{-}pinh)N_3\ H_2O]_n$ (**1**) nano-cauliflower

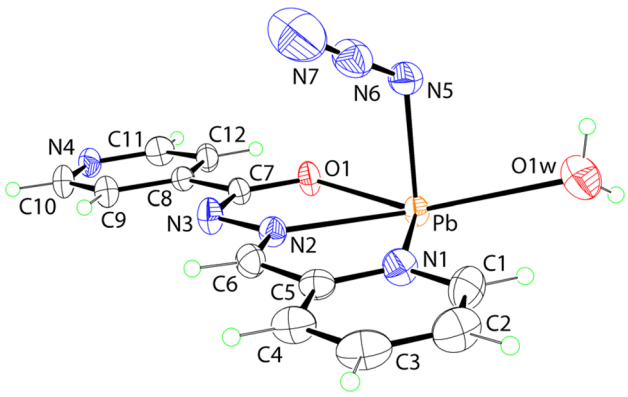

Fig. 4 Molecular structure of the asymmetric unit of $[Pb(\mu\text{-}2\text{-}pinh)N_3(H_2O)]_n$ with atom labelling

Table 1 Crystal data and refinement details for $[Pb(\mu\text{-}2\text{-}pinh)N_3(H_2O)]_n$

Empirical formula	$C_{12}H_{11}N_7O_2Pb$
Formula weight	492.47
Crystal system	orthorhombic
Space group	*Pbcn*
a (Å)	12.6325 (10)
b (Å)	16.5639 (13)
c (Å)	13.7687 (11)
Volume (Å^3)	2881.0 (4)
Z	8
ρ_{calc}/mg mm^{-3}	2.271
μ/mm^{-1}	11.731
F (000)	1840
Crystal size (mm^3)	0.10 × 0.20 × 0.40
2θ range for data collection (°)	4.0–55.0
Reflections collected	25,636
Independent reflections	3312 [R(int) = 0.067]
Data with I ≥ 2σ(I)	2238
Goodness-of-fit on F^2	1.01
Final R indexes (obs. data)	R_1 = 0.026, wR_2 = 0.056
Final R indexes (all data)	R_1 = 0.059, wR_2 = 0.070
Largest diff. peak/hole (e Å^{-3})	1.12/−1.01

H1w2 = 162° for symmetry operation ½ − x, ½ − y, ½ + z). The second water-bound hydrogen does not form a strong hydrogen bond but instead lies in the region defined by two terminal N7 atoms of the azide ligand (H···N7^{iii} = 2.66 Å and H···N7^{iv} = 2.76 Å for iv: ½ + x, ½ − y, 1 − z).

This arrangement suggests a gap or hole in the coordination geometry around the metal ions, which is possibly occupied by a stereo-active lone pair of electrons on lead(II) [12]. This possibility is supported by the observed shortening of the Pb–N bonds on the side of the Pb^{2+} ion opposite to the putative lone pair [2.347(6) Å compared with 2.944(5) Å adjacent to the lone pair] [10]. Such an environment leaves space for close contact with another atom (Fig. 7). To find any potential donor centre, it is necessary to extend the bonding limit. If a limit of 3.30 Å is placed on the separation of Pb^{II} donor atoms that are regarded as being involved in coordination bonding, the Pb1 atoms are in close contact with the nitrogen atom of the 2-pinh ligand in a parallel chain with distances of Pb1···N3^i = 3.511 Å. The Pb···Pb separation in the chain is 9.973 Å, and the Pb···Pb separation in the zig-zag pattern is 13.769 Å.

There are some noncovalent π–π stacking interactions [36] between the parallel aromatic rings of the adjacent

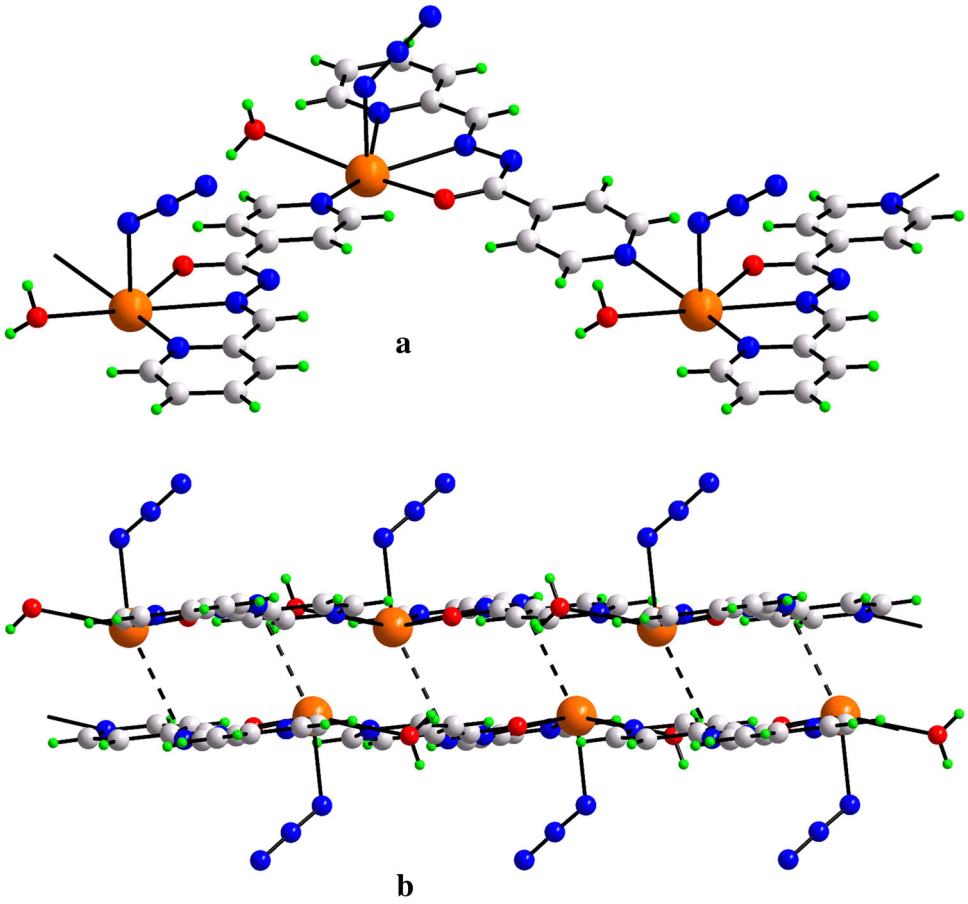

Fig. 5 **a** Fragment of the coordination polymer showing the 1D zigzag polymeric chain. **b** Association between chains related by twofold symmetry via Pb···N3 interactions

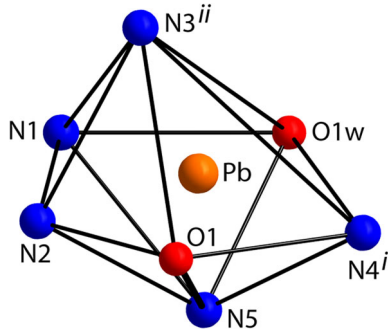

Fig. 6 Immediate environment of lead atom in **1**. Bond lengths [Å]: Pb–O1 = 2.404(4), Pb–O1w = 2.944(5), Pb–N1 = 2.796(5), Pb–N2 = 2.546(4), Pb–N5 = 2.347(6), Pb–$N4^{i}$ = 2.706(5), Pb···$N3^{ii}$ = 3.283(5). Symmetry operation i: x, 1 − y, ½ + z and ii: 1 − x, y, ½ − z

chains, as shown in Figs. 8 and 9. The interplanar distance of the aromatic rings (Fig. 8) is 3.965 Å, which is appreciably shorter than the normal π–π stacking [37]. Consequently, the π–π stacking interactions also allow the 1D zig-zag structure to form a 3D network (Fig. 9). Thus, lone pair activity and π–π stacking may control the coordination sphere of lead(II) ions in this complex. The obvious question then is whether the lone pair activity has stretched coordinate bonds, which would result in ligand stacking, or whether it is the stacking interaction, which results in donor atoms forming a gap in the coordination sphere. However, there could be a cooperative effect of the π–π interactions and the presence of the lone pair in producing closer packing of the structure.

PbO nano powders have been prepared by thermolysis of **1** at 180 °C with oleic acid as a surfactant. The powder XRD patterns (Fig. 10) match with the standard pattern of orthorhombic PbO with $a = 5.8931$ Å and $z = 4$ (JCPDS card file No. 77-1971), which confirms the formation of PbO powder. The significant broadening of the peaks of the nanostructure indicates that the particles have nanometer dimensions. The average size of the particles was estimated using the Scherrer formula as 30 nm (comparable with TEM and SEM). morphology and size of the PbO samples were further investigated using SEM and TEM. The bulk powder of **1** produces regularly shaped Pb(II) oxide nanoparticles with diameter of about 30 nm (Figs. 11, 12), which is compatible with similar reported processes [38–40].

Thermo-gravimetric (TG) and differential thermal analyses (DTA) were performed on complex [Pb(μ-2-

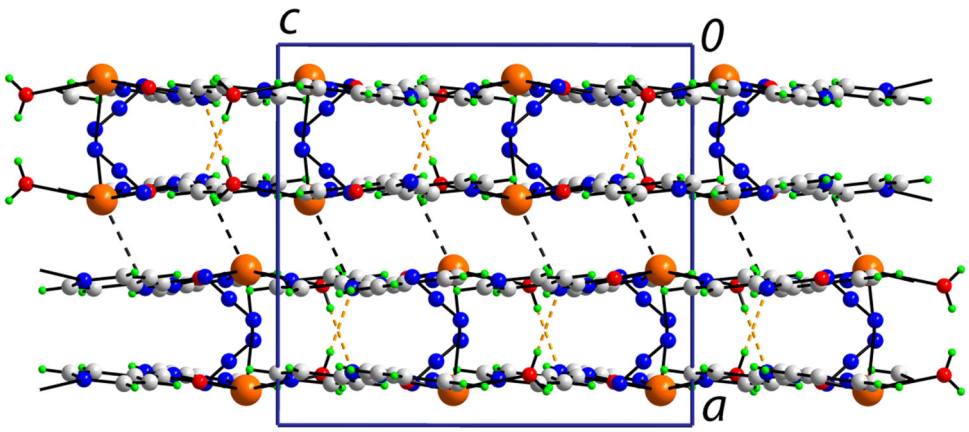

Fig. 7 Unit cell contents of **1** shown in projection down the b-axis highlighting the stacking of layers along the a-axis

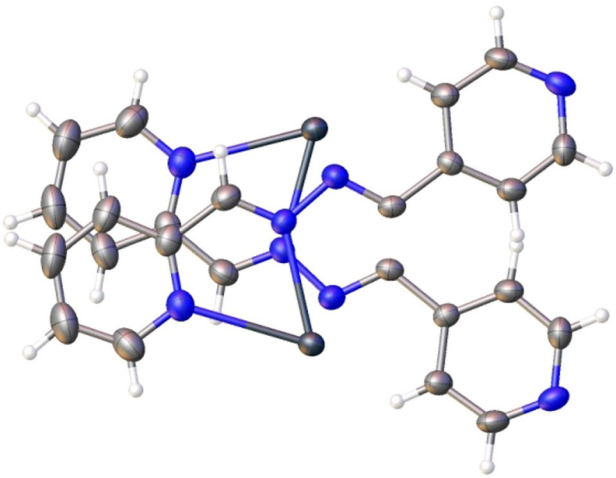

Fig. 8 Projection of the nearest neighbor pairs of π–π stacks of heteroaromatic bases in $[Pb(\mu\text{-}2\text{-}pinh)N_3(H_2O)]_n$

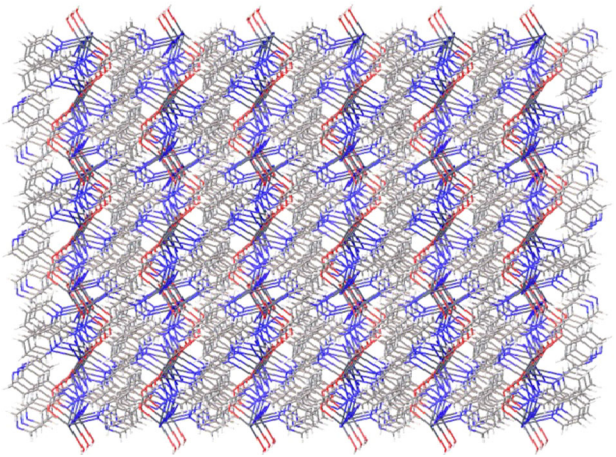

Fig. 9 Packing of 1D zig-zag chains forming 3D supramolecular layers via π–π stacking interactions

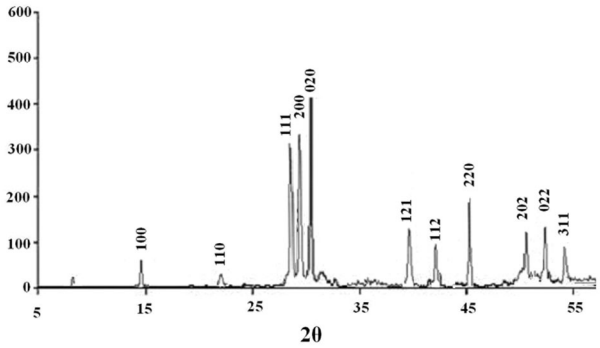

Fig. 10 XRD patterns of PbO after calcination of **1**

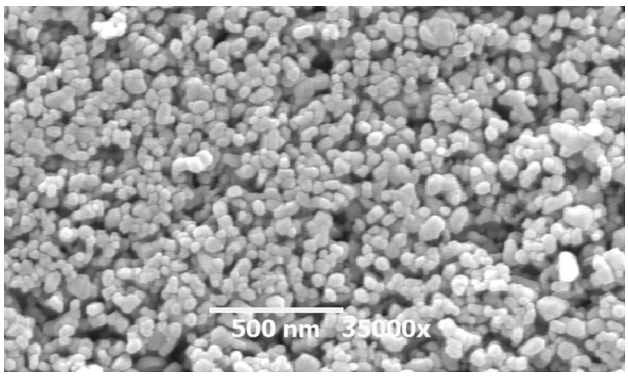

Fig. 11 SEM image of PbO nano-powder (produced by calcination of nano-cauliflower)

pinh)N_3 $H_2O]_n$ (**1**) at 25 to 800 °C under a nitrogen atmosphere (Fig. 13). The complex dehydrates between 62 and 149 °C with a mass loss of 3.6 % (calcd. 3.7 %), and the anhydrous compound melts at 174 °C. Then, the simultaneous removal of both N3 and the 2-pinh ligand is observed exothermically in the range of 200–494 °C, leading to the formation of PbO. The corresponding mass

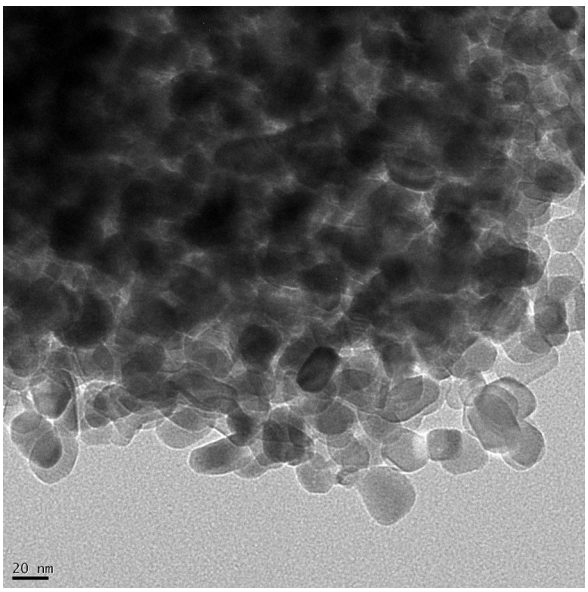

Fig. 12 TEM image of PbO nano-powder (produced by calcination of nano-cauliflower)

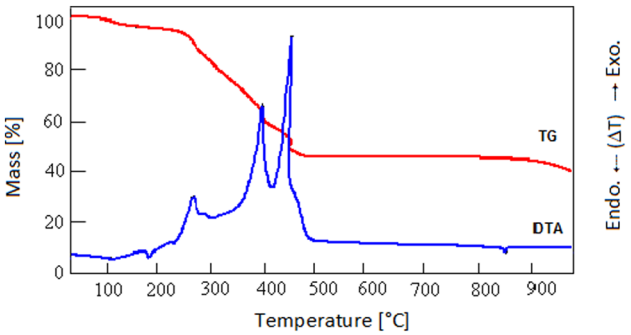

Fig. 13 Thermal analysis of complex (**1**): TG and DTA curves

loss of 52.5 % is consistent with the calculated value of 54.2 %. Melting of PbO occurs at ca. 850 °C.

2.1 NBO Analysis

The NBO analysis shows the total natural charge of lead atoms (1.39 for Pb1). The positively charged Pb(1) atom is closely surrounded by four electronegative atoms: O2, N3, N4, and N7, which have natural charges of −0.830, −0.587, −0.410, and −0.729, respectively. The electronic properties of the Pb(1) atom are well characterized by second-order perturbation theory analysis of the Fock matrix and demonstrate that antibonding lone pairs of lead are strongly electron donating due to the N_3 group. The NBO analysis indicated 79 stabilization interactions over a threshold of 0.50 kcal/mol between filled Lewis-type NBOs of the azide group (donor) and formally empty non-Lewis NBO of the Pb1 atom (acceptor). The total second-order stabilization energy $E^{(2)}$ is 115.7 kcal/mol, which is calculated as the sum of $E^{(2)}$ for alpha and beta spin orbitals.

Critical roles are played in stabilizing the chemical structure by the three interactions listed in Table 2 between the donor lone pair orbital on the nitrogen atom LP(N7) and the acceptor lone pair antibonding orbital on the lead atom (LP(N7) → LP*(Pb1)). N7-Pb1 interaction is also responsible for breaking the D_{2h} symmetry of the linear azide group and the difference between the N7–N8 and N8–N9 distances. The presence of an electron-positive lead atom closer to the nitrogen N7 results in inequality of the natural charge of peripheral nitrogen atoms (−0.73 for N7 and −0.19 for N9). It also results in asymmetric electronic structure of the azide group (for example, asymmetric NBO bond arrangement: only one $\sigma_{N7–N8}$ bond versus one $\sigma_{N8–N9}$ plus two $\pi_{N8–N9}$ bonding orbitals).

Interactions between lone pairs of N3, N4, and O2 atoms with respective antibonding lone pairs of Pb1 give the strongest stabilization effect (see Table 3). Therefore, lead is finely fixed on its position. Other stabilizing interactions have much less energetic importance, such as $\sigma_{O2–C21}$ → LP4*(Pb1), LP1(N32) → LP4*(Pb1), and $BD_{N5–C19}$ → LP3*(Pb1). The NBO orbitals involved in donor–acceptor interaction with Pb1 are shown as rendered spheres in Fig. 14. It should be noted that antibonding lone pairs of Pb1 have positive but very low energy (only 0.0004–0.04 a.u.). Therefore, they have relatively high occupancy (e.g., 0.3*e* for LP2*Pb1) and play an important role in the delocalization effect.

The total steric exchange energy [41] arises almost entirely from the organic unit. About 2 % of the total steric energy is delivered by LP1(Pb1) NLMO (natural localized molecular orbital; Table 3).

3 Conclusions

A novel lead(II) coordination polymer containing a terminal azide anion, $[Pb(\mu\text{-}2\text{-pinh})N_3\ H_2O]_n$ (**1**), was synthesized by a simple sonochemical preparation method. This coordination polymer can be used in the preparation of PbO nanoparticles. The crystal structure of the complex forms a one-dimensional zig-zag polymer in solid state. The arrangement of the ligands suggests a gap in the coordination geometry around the metal ions, which is possibly occupied by a stereo-active lone pair of electrons on lead(II). Lone pair activity and π–π stacking may control the coordination sphere of lead(II) ions in this complex.

A new theoretical method was used to examine the electronic structure and determine the electronic properties

Table 2 Second-order interaction energy (E^2, kcal/mol) between donor → acceptor orbitals (the molecular units found in the alpha and beta manifolds are not equivalent)

Donor → acceptor (LP = lone pair; BD = natural bond orbital)	Second-order interaction energy (E^2, kcal/mol)	
	Alpha spin orbitals	Beta spin orbitals
LP1 (N7) → LP3*Pb(1)	17.23	17.86
LP2 (N7) → LP2*Pb(1)	17.90	16.97
LP1 (N7) → LP2*Pb(1)	11.66	11.96
LP2 (O2) → LP4*Pb(1)	13.46	13.29
LP1 (N4) → LP2*Pb(1)	17.77	18.08
LP1 (N3) → LP4*Pb(1)	7.79	7.74
LP1 (N6) → LP2*Pb(31)	23.00	–
LP1 (N6) → LP3*Pb(31)	–	24.47
$BD^*_{N4\text{-}Pb31}$ → $BD_{N4\text{-}Pb31}$	–	34.54
$BD^*_{N4\text{-}Pb31}$ → $BD_{N5\text{-}C19}$	–	254.79

Table 3 Steric exchange energy calculated by units

Unit	Steric exchange energy ($E^{NLMO}_{exchange}$, kcal/mol)	
	Alpha spin orbitals	Beta spin orbitals
Pb1	16.07	15.95
Organic unit	713.68	745.19
N_3 group	65.60	58.71
N32	2.30	0.43
Total steric exchange energy	804.22	843.27

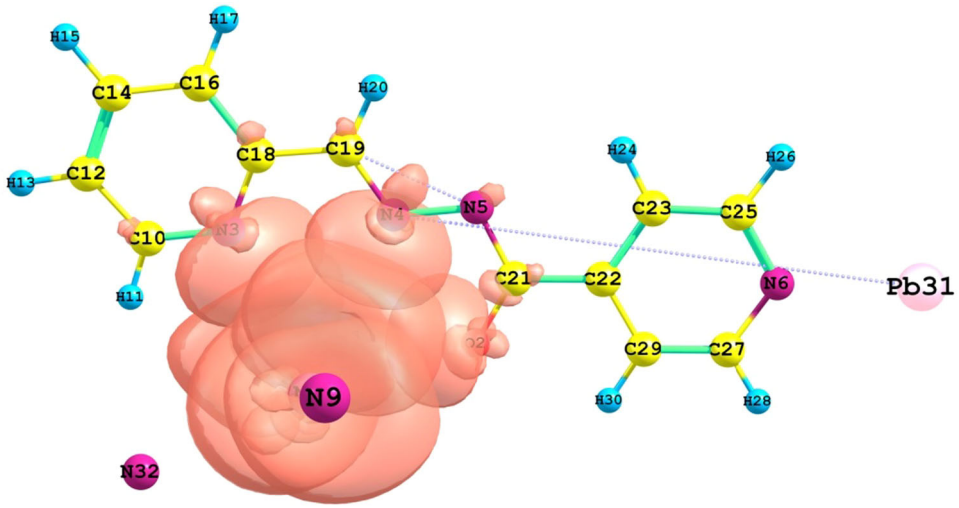

Fig. 14 Donor-acceptor (bonding-antibonding) interaction of lead atoms

of lead atoms. The electronic properties of the Pb(1) atom were well characterized by second-order perturbation theory analysis of the Fock matrix, which demonstrated that antibonding lead lone pairs are strongly electron-donating due to the N_3 group. Three interactions between the donor lone pair orbital on the nitrogen atom (LP(N7)) and the acceptor lone pair antibonding orbital on the lead atom (LP(N7) → LP*(Pb1)) play a critical role in stabilizing the chemical structure. Also, interactions between lone pairs of N3, N4, and O2 atoms with respective antibonding lone pairs of Pb1 give the strongest stabilization effect, which result in lead being finely fixed on its position. Antibonding lone pairs of Pb1 have positive but very low energy (only 0.0004–0.04 a.u.). Therefore, they have relatively high occupancy (e.g., 0.3*e* for LP2*Pb1) and play an important role in the delocalization effect.

4 Experimental Section

4.1 Materials and Physical Measurements

The 2-pyridinecarbaldehyde isonicotinoylhy-drazone (H-2-pinh) ligand was synthesized according to a literature method [42]. All other chemicals were obtained from commercial sources and used without further purification. Ultrasound was applied using a multiwave ultrasonic generator (Sonicator_3000; Misonix Inc., Farmingdale, NY, USA), which was equipped with a converter/transducer and titanium oscillator (horn; 12.5-mm diameter). The generator was operated for 1 h at 20 kHz with a maximum power output of 600 W and at room temperature. Infrared spectra were recorded using KBr pellets with a Perkin-Elmer 883-IR spectrophotometer and a Nicolet 520 FTIR spectrophotometer. Elemental analyses (C, H, N) were performed on a Perkin-Elmer 2400 II elemental analyser. X-ray powder diffraction (XRD) measurements were performed with monochromatized Cuk_{α} radiation using an X'pert diffractometer manufactured by the Panalytical company. Simulated XRD powder patterns based on single-crystal data were prepared using the Mercury program [43].

The crystallite sizes of selected samples were estimated using the Scherrer formula. The samples were characterized using a scanning electron microscope and gold coating. Melting points were measured on an Electrothermal 9100 apparatus and are uncorrected. Thermal analysis curves (TG and DTA) were obtained using a Seiko Exstar TG/DTA 6200 thermal analyser in a nitrogen flow with a heating rate of 10 K min^{-1}. The sample size was 5–10 mg, and platinum crucibles were used.

4.2 Preparation of $[Pb(\mu\text{-}2\text{-}pinh)N_3\ H_2O]_n$

To prepare the nano-structure of $[Pb(\mu\text{-}2\text{-}pinh)N_3\ H_2O]_n$ (**1**), a high-density ultrasonic probe was placed in 15 mL of a 0.1 M solution of $Pb(CH_3COO)_2$ in H_2O/MeOH and operated at 20 kHz with a maximum power output of 600 W. To this solution, 15 mL of 0.1 M H-2-pinh ligand solution and 15 mL of 0.1 M sodium azide solution were added dropwise. The obtained precipitates were filtered off, washed with water, and dried in air.

Product 1: m.p. = 173 °C. Analysis: Found; C: 30.00, H: 2.20, N: 20.00 %. calcd. for $C_{12}H_{11}N_7O_2Pb$: C: 29.27, H: 2.25, N: 19.91 %.

IR (selected bands; in cm^{-1}): 700 *s*, 761 *m*, 855 *m*, 1024 *m*, 1151 *m*, 1350 *s*, 1463 *m*, 1576 *m*, 1603 *m*, 2021*vs*, 2923 *m*, 3423*br* cm^{-1} [35].

To isolate single crystals of $[Pb(\mu\text{-}2\text{-}pinh)N_3\ H_2O]_n$ (**1**), H-2-pinh (0.23 g, 1 mmol) was placed in one arm of a branched tube, while $Pb(CH_3COOH)_2$ (0.32 g, 1 mmol) and sodium azide (0.07 g, 1 mmol) were placed in the other. Methanol was then carefully added to fill both arms, and the tube was sealed. The ligand-containing arm was immersed in a bath at 60 °C, while the other arm was left at ambient temperature. After 2 weeks, crystals (m.p. 175 °C) suitable for X-ray structure determination were deposited in the arm kept at ambient temperature. They were then filtered off, washed with acetone and ether, and air dried (yield: 73 %). Analysis: Found; C: 29.20, H: 2.20, N: 19.80 %. calcd. for $C_{12}H_{11}N_7O_2Pb$: C: 29.27, H: 2.25, N: 19.91 %).

IR (selected bands; in cm^{-1}): 699 *s*, 761 *m*, 854 *m*, 1023 *m*, 1149 *m*,13509 *s*,1461 *m*, 1565 *m*, 1601 *m*, 2023*vs*, 2923 *m*, 3419*br* cm^{-1} [35].

4.3 Crystallography

Crystallographic data were collected at 298(2) K with an Oxford Xcalibur CCD area detector diffractometer using graphite monochromatic Mo Kα radiation ($\lambda = 0.71069$ Å). Data reduction and absorption correction were performed using CrysAlis RED 1.171.26 (Oxford diffraction). The structure was solved by direct methods using SIR2004 [44] and refined by full-matrix least squares using SHELX-97 [44]. Hydrogen atoms were generated in the calculated positions using SHELX-97 [45]. Materials for publication were prepared using SHELXTL [45], ORTEPIII [46], and Olex2 [47]. The crystallographic data for the structures were deposited at the Cambridge Crystallographic Data Centre as supplementary publication CCDC-1442406 for $[Pb(\mu\text{-}2\text{-}pinh)N_3\ H_2O]_n$ (**1**). Copies of the data can be obtained upon request from CCDC, 12 Union Road, Cambridge CB2 1EZ, UK [Fax: +44-1223-336033; E-mail: de-posit@ccdc.cam.ac.uk].

4.4 Theoretical Methods

The NBO analysis was performed using the standalone NBO program version 5.0 [48]. NBO version 3.1 is implemented in the Gaussian 98, 03, and 09 packages and produces very similar natural bond analysis results compared with the new version of the NBO program. However, NBO 5.0 is much more detailed when describing the electronic structure. For example, it can illustrate the localized NBO/NLMO contributions to the steric exchange energy [49].

Acknowledgments Support from the University of Qom is gratefully acknowledged. This work was funded by Grant NRF-2015-002423 of the National Research Foundation of Korea. The theoretical calculations were financed by a statutory activity subsidy from the Polish Ministry of Science and Higher Education for the Faculty of Chemistry of Wrocław University of Technology. DB acknowledge

generous computer time from the Wrocław Supercomputer and Networking Center.

References

1. R. Chakrabarty, P.S. Mukherjee, P.J. Stang, Chem. Rev. **111**, 6810–6918 (2011)
2. A. Erxleben, Coord. Chem. Rev. **246**, 203–228 (2003)
3. C.L. Cahill, D.T. de Lill, M. Frisch, CrystEngComm **9**, 15–26 (2007)
4. A. Morsali, L.-G. Zhu, Helv. Chim. Acta **89**, 81–93 (2006)
5. S.R. Batten, S.M. Neville, *Coordination Polymers: Design, Analysis and Application*, vol. 89 (The Royal Society of Chemistry, Cambridge, 2009)
6. C. Janiak, Dalton Trans. **14**, 2781–2804 (2003). doi:10.1039/B305705B
7. H. Li, J. Zhai, X. Sun, RSC Adv. **1**, 725–730 (2011)
8. K. Kavallieratos, J.M. Rosenberg, J.C. Bryan, Inorg. Chem. **44**, 2573–2575 (2005)
9. L.F. Lindoy, Pure Appl. Chem. **69**, 2179 (1997)
10. R.D. Hancock, A.E. Martell, Chem. Rev. **89**, 1875 (1989)
11. L.M. Engelhardt, B.M. Furphy, J.M. Harrowfield, J.M. Patrick, A.H. White, Inorg. Chem. **28**, 1410 (1989)
12. L. Shimonni-Livny, J.P. Glusker, C.W. Bock, Inorg. Chem. **37**, 1853 (1998)
13. J.S. Casas, J. Sordo, *LEAD, chemistry, analytical aspects, environmental impact and health effects*, 1st edn. (Elsevier, Boston, 2006)
14. A. Walsh, G.W. Watson, J. Solid State Chem. **178**, 1422 (2005)
15. N. Soltanzadeh, A. Morsali, Ultrason. Sonochem. **17**, 139–144 (2010)
16. H. Sadeghzadeh, A. Morsali, CrystEngComm **12**, 370–372 (2010)
17. V. Safarifard, A. Morsali, Coord. Chem. Rev. **292**, 1–14 (2015)
18. S.M. Soliman, J. Mol. Struct. **1048**, 308–320 (2013)
19. S.M. Soliman, T.S. Kassem, A.M.A. Badr, M.A. Abu Youssef, R. Assem, J. Mol. Struct. **2014**, 168–179 (1074)
20. M. Nora, M. Fatiha, N. Leila, H. Sakina, K. DjamelEddin, J. Mol. Liq. **211**, 40–47 (2015)
21. Z.K. Eddine, M. Fatiha, Z. Amal, N. Leila, M. Rachid, C. R. Chimie **18**, 193–198 (2015)
22. B. Shaabani, B. Mirtamizdoust, D. Viterbo, G. Croce, H. Hammud, P. Hojati-Lalemi, A. Khandar, Z. Anorg. Allg. Chem. **637**, 713–719 (2011)
23. B. Mirtamizdoust, B. Shaabani, S.W. Joo, D. Viterbo, G. Croce, Y. Hanifehpour, J. Inorg. Organomet. Polym. **22**, 1397–1403 (2012)
24. B. Shaabani, B. Mirtamizdoust, M. Shadman, H.K. Fun, Z. Anorg. Allg. Chem. **635**, 2642–2647 (2009)
25. B. Mirtamizdoust, B. Shaabani, A. Khandar, H.K. Fun, S. Huang, M. Shadman, P. Hojati-Talemi, Z. Anorg. Allg. Chem. **638**, 844–850 (2012)
26. Y. Hanifehpour, B. Mirtamizdoust, S.W. Joo, J. Inorg. Organomet. Polym. **22**, 916–922 (2012)
27. Y. Hanifehpour, B. Mirtamizdoust, A.R. Farzam, S.W. Joo, J. Inorg. Organomet. Polym. **22**, 957–962 (2012)
28. B. Mirtamizdoust, S. Ali-Asgari, S.W. Joo, E. Maskani, Y. Hanifehpour, T.H. Oh, J. Inorg. Organomet. Polym. **23**, 751–757 (2013)
29. Y. Hanifehpour, A. Morsali, B. Mirtamizdoust, S.W. Joo, J. Mol. Struct. **1079**, 67–73 (2015)
30. B. Mirtamizdoust, M.S. Shalamzari, S. Behrouzi, M.H. Florencio, H.K. Fun, J. Inorg. Organomet. Polym. **22**, 1358–1364 (2012)
31. Y. Hanifehpour, B. Mirtamizdoust, A. Morsali, S.W. Joo, Ultrason. Sonochem. **23**, 275–281 (2015)
32. Y. Hanifehpour, V. Safarifard, A. Morsali, B. Mirtamizdoust, S.W. Joo, Ultrason. Sonochem. **23**, 282–288 (2015)
33. Y. Hanifehpour, B. Mirtamizdoust, B. Khomami, S.W. Joo, Z. Anorg, Allg. Chem. **641**, 2466–2472 (2015)
34. J.M. Harrowfield, H. Miyamae, B.W. Skelton, A.A. Soudi, A.H. White, Aust. J. Chem. **49**, 1165 (1996). **and references therein**
35. L.K. Nakamoto, *Infrared and Raman spectra of inorganic and coordination compounds*, 5 Part B edn. (Wiley, New York, 1997), pp. 124–126
36. N.N. Greenwood, A. Earnshaw, *Chemistry of the Elements* (Pergamon Press, Oxford, 1986), pp. 235–254
37. C.A. Hunter, J.K.M. Sanders, J. Am. Chem. Soc. **112**, 5525–5534 (1990)
38. K. Akhbari, A. Morsali, CrystEngComm **13**, 2047 (2011)
39. L. Hashemi, A. Morsali, P. Retailleau, Inorg. Chim. Acta **367**, 207 (2011)
40. H. Sadeghzadeh, A. Morsali, Ultrason. Sonochem. **18**, 80 (2011)
41. J.K. Badenhoop, F. Weinhold, J. Chem. Phys. **107**(5406–5421), 5422–5432 (1997)
42. C.M. Armstrong, P.V. Bernhardt, P. Chin, D.R. Richardson, Eur. J. Inorg. Chem. **2003**, 1145 (2003)
43. Mercury 2.4, Copyright Cambridge Crystallographic Data Centre, 2001–2010
44. A. Altomare, M.C. Burla, M. Camalli, G.L. Cascarano, C. Giacovazzo, A. Guagliardi, A.G. Moliterni, G. Polidori, R. Spagna, J. Appl. Crystallogr. **32**, 115–119 (1999)
45. G.M. Sheldrick, A short history of SHELX. Acta Crystallogr. A **64**(1), 112–122 (2007)
46. L.J. Farrugia, J. Appl. Crystallogr. **30**, 565 (1997)
47. O.V. Dolomanov, L.J. Bourhis, R.J. Gildea, J.A.K. Howard, H. Puschmann, J. Appl. Cryst. **42**, 339–341 (2009)
48. NBO 5.0., E. D. Glendening, J. K. Badenhoop, A. E. Reed, J. E. Carpenter, J. A. Bohmann, C. M. Morales, and F. Weinhold (Theoretical Chemistry Institute, University of Wisconsin, Madison, WI, 2001); http://www.chem.wisc.edu/∼nbo5
49. J.K. Badenhoop, F. Weinhold, Int. J. Quantum Chem. **72**, 269–280 (1999)
50. A. Angelova, B. Angelov, R. Mutafchieva, S. Lesieur, J. Inorg. Organomet. Polym. **25**, 214–232 (2015)
51. N.N. Gubanova, G.P. Baranchikov, L. Kopitsa, L. Almásy, Y. Ye, L.B. Angelov, A.D. Yapryntsev, L. Rosta, V.K. Ivanov, Ultrason. Sonochem. **24**, 230–237 (2015)
52. B. Angelov, A. Angelova, M. Drechsler, V.M. Garamus, R. Mutafchieva, S. Lesieur, Soft Matter **11**, 3686–3692 (2015)